Land Subsidence Detected by Persistent Scatterer Interferometry Using ALOS/PALSAR Data from the Nakagawa Lowland in the Central Kanto Plain, Japan

Shoichi Hachinohe and Yu Morishita

Abstract

The Nakagawa lowland is located in the central part of the Kanto Plain; the largest plain in Japan. During the 1960s, major land subsidence occurred, exceeding 10 cm/year, as a result of over pumping of shallow and deep groundwaters in this area. In recent times, following the regulation of pumping by national and local governments, the amount of land subsidence in this area has decreased sharply. However, in the Nakagawa lowland, subsidence exceeding 1 cm/year is still ongoing in some areas, and is more pronounced during dry years in which the amount of groundwater use increases. In this study, we examined the local characteristics of land subsidence through persistent scatterer interferometry using ALOS/PALSAR data obtained from April 2006 to April 2011. On the basis of this analysis, we confirmed that subsidence was concentrated along the western margin of an incised buried valley, in which average displacement rates exceed 10 mm/year. The characteristics of this subsidence zone are suggestive of a geological structure that is buried beneath the alluvial plains, which is affected by groundwater pumping that targets the basal gravel layers of buried valley-fills. In addition, we detected a patched zone of around 0.3 km^2 in the study area, in which average displacement rates exceed 15 mm/year. We estimated that this zone was formed by consolidation settlement of soft ground as a result of residential landfill.

Keywords

Alluvial plain • ALOS/PALSAR • Incised buried valley • Land subsidence • SAR interferometry

1   Introduction

In the fifth assessment report of the intergovernmental panel on climate change [IPCC 2013], the generation of extreme weather was predicted to accompany ongoing global warming. In the Kanto district of Japan, which contains around 30% of the country's population, it has also been proposed that climate change will not only generate an unexpected scale of torrential rainfall, but also extensive water shortages as a result of specific dry weather conditions that are now more frequent [Japan Meteorological Agency 2013]. When an extensive water shortage occurs, the water supplied by rivers is substantially decreased, and so the amount of extracted groundwater increases. Various studies have shown a spatial and temporal correlation between water pumping and land subsidence [*e.g.* Constan et al. 2016; Ishitsuka et al. 2014; Ferretti et al. 2000]. During previous decades, whenever water shortages have occurred in the Kanto district, the land subsidence area has experienced broad expansion [Morita 2015]. Thus, it may be expected that, if large-scale water shortages occur again in the

S. Hachinohe (✉)
Research Institute, Center for Environmental Science in Saitama, Kazo, Saitama, Japan
e-mail: hachinohe.shoichi@pref.saitama.lg.jp

Y. Morishita
Geospatial Information Authority of Japan, Tsukuba, Ibaraki, Japan

Fig. 1 Location of the study area and Saitama prefecture on a topography map of Kanto district
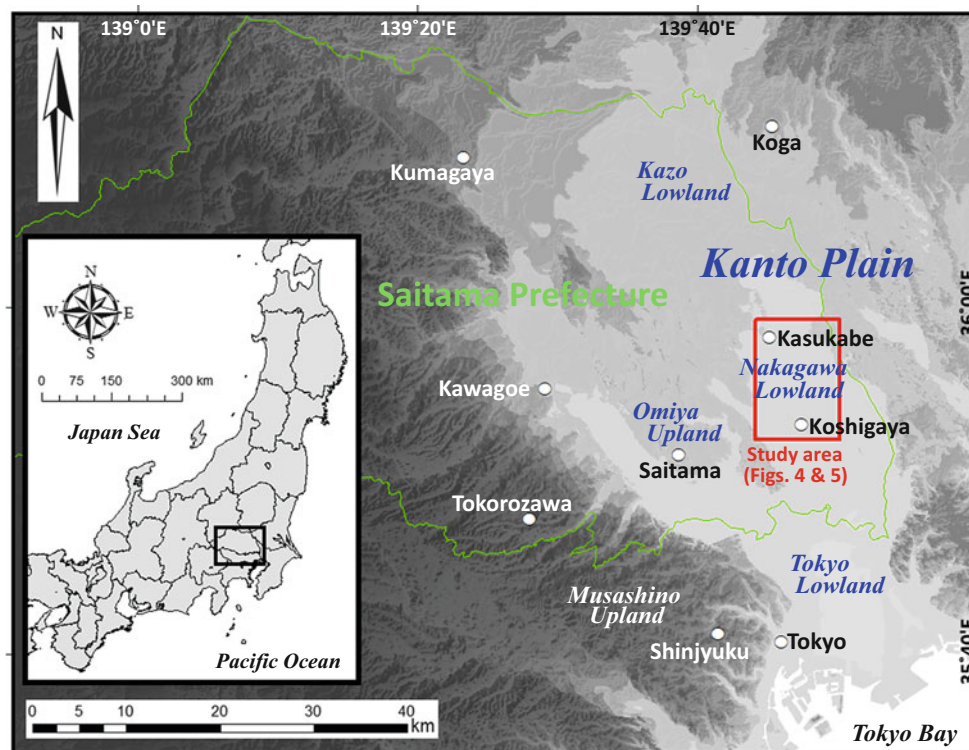
near future, a similar amount, or even larger scale of land subsidence may be seen in this area.

In recent years, analyses of land surface displacements through remote sensing using data from satellites and aircraft have made significant contributions to various fields, including the earth sciences [*e.g.* Bekaert et al 2015; Hooper et al 2012; Zebker et al. 1994] and disaster prevention [*e.g.* Ozawa and Fujita 2013]. In particular, as a result of the improvements in quantities and qualities of data obtained by Synthetic Aperture Radar (SAR) and the establishment of correction methods various types of errors, scientists have been able to precisely detect the movement of land surface. In this research, in order to evaluate the local characteristics of land subsidence in the Nakagawa lowland (Fig. 1), in which the likelihood of land subsidence is high during water shortages in the near future, we perform and examine persistent scatterer interferometry (PSI) using ALOS PALSAR (L-band) SAR data acquired by JAXA.

2   Study Area

Land subsidence became a major problem in almost all the alluvial plains in Japan after World War II, due to an increase in the amount of groundwater extraction that occurred in line with the economic recovery. The Tokyo bayside region has experienced the most significant land subsidence over the past 80 years, with the total subsidence having exceeded 4 m by 1970 [Endo 2009]. In the Kanto plain (Fig. 1), various types of pumping regulations have been imposed by national and local governments since the 1950s. Under these restrictions, groundwater levels in this area recovered dramatically from the end of the 1960s to the early 1970s, while land subsidence rates also improved [Hachinohe et al. 2014]. However, the areas in which the land subsidence was concentrated shifted from Tokyo city center to suburban areas, including the Kazo lowland, the Musashino upland [Hayashi 2004]. Therefore, it appears that these phenomena have been produced by the movement of concentrated groundwater use from the southern part of the Kanto plain to the surrounding satellite cities, as a result of the expansion of urbanization.

Figure 2a shows the distribution of annual land subsidence in Saitama prefecture, north of Tokyo, in 1975, as shown by leveling measurements. As shown in this figure, we can confirm that land subsidence is concentrated in the Kazo lowland, the Musashino upland, the Nakagawa lowland and the Omiya upland (Figs. 1 and 2). Although the subsidence trends become less pronounced over time, as shown in Fig. 2b, c, subsidence in the Kazo lowland and the Nakagawa lowland is still ongoing. The land subsidence in the Nakagawa lowland has been detected through SAR observations by Tobita et al. 2005 and Deguchi et al. 2009. Tobita et al. 2005 measured a maximum vertical subsidence

Fig. 2 Changes in land subsidence areas and annual subsidence in Saitama prefecture, north of Tokyo, Japan [from Hachinohe et al. 2014]
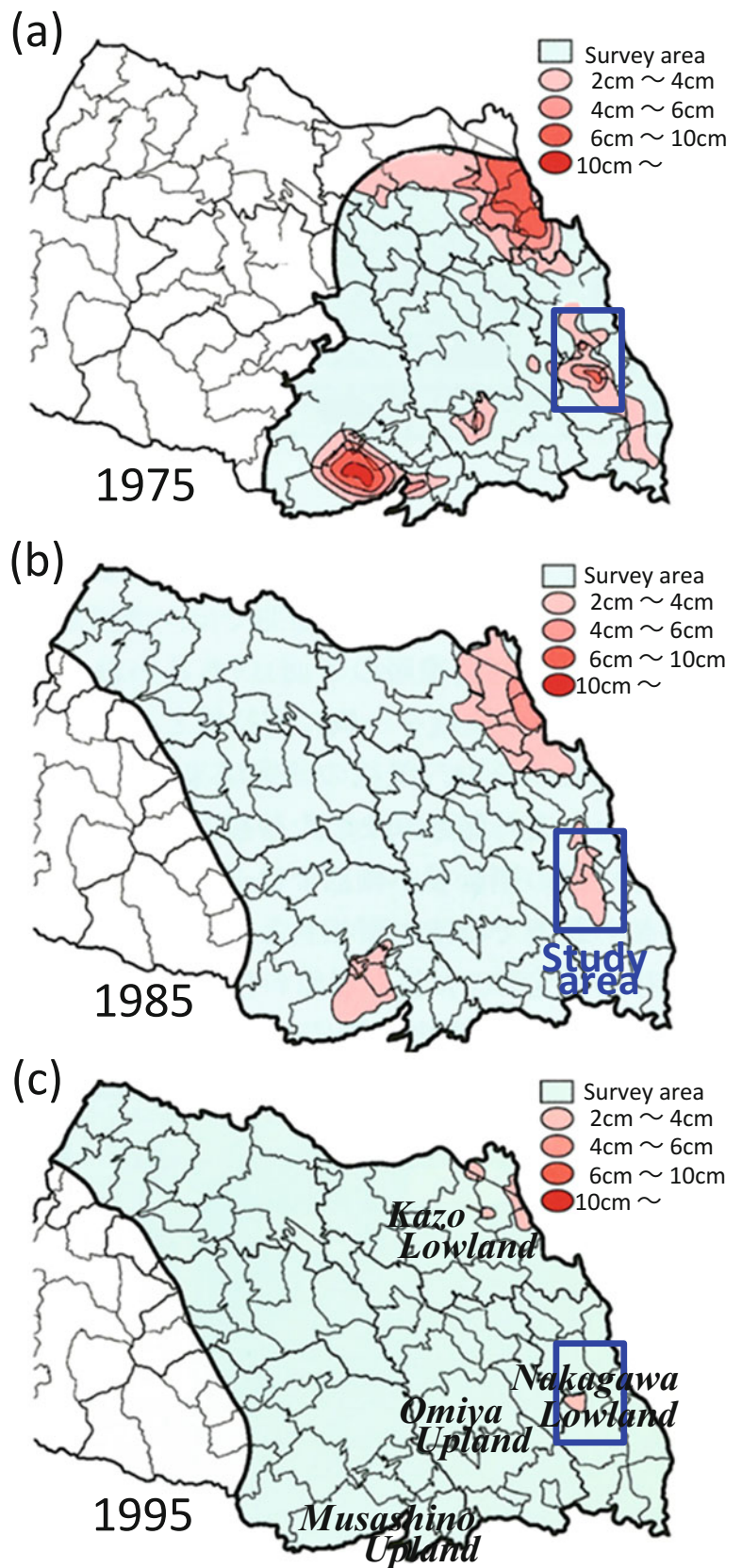
of around 4 cm over about 3 years from January 1995 to March 1998, using JERS-1 and GPS positioning data. Deguchi et al. 2009 measured a maximum line-of-sight (LOS) displacement of around 5 cm over five and a half years from January 2003 to June 2008 using ENVISAT data.

3 SAR Methodology

The Japan Aerospace Exploration Agency (JAXA) launched their Advanced Land Observing Satellite (ALOS) in 2006, and observational data were obtained up until 2011. In this study, we carried out persistent scatterer interferometry (PSI) by DORIS [Kampes et al. 2003] and StaMPS/MTI [Hooper et al. 2012] within the Nakagawa lowland using SAR data from ALOS. The PSI method is an analytical technique that allows the calculation of rates of displacement of a target on the land surface through the extraction of points that have stable phase characteristics over time (PS), such as roads and buildings. As an external digital elevation model (DEM), we used Base map information with an interval of 10 m which is constructed and distributed in free by Geospatial Information Authority of Japan (GSI) (http://fgd.gsi.go.jp/download/menu.php). SAR can detect only one-dimensional displacements between the satellite and a target on the land surface in the direction of the LOS. However, in satellite-based SAR observations, it is possible to observe the same location on the Earth's surface from the two directions of the ascending and the descending orbits. We can calculate quasi-vertical and quasi-east–west components of a displacement rate on a plane determined by ascending and descending LOS vectors from the two LOS displacement rates (Fig. 3) [Fujiwara et al. 2000; Kobayashi et al. 2015; Huang et al. 2016]. For this study area, ALOS/PALSAR data exist on paths 405 and 406 of the ascending orbit and path 58 of the descending orbit, with the data sets of each path comprising 24, 22 and 23 images, respectively (Table 1). We first calculated average displacement rates in the LOS direction using the data sets from these three paths, for 4 years from 2007 to 2010. A huge number of PS points were detected in this area, and so we thinned out the data at 200 m-intervals before analysis [*e.g.* Fujiwara et al. 2000]. Tropospheric noise reduction using a numerical weather model provided by Japan Meteorological Agency (JMA) was applied [Kobayashi et al. 2014]. In order to reduce the influences of any orbital errors, a correction to flatten the phase inclination of the entire study area was applied. The average of the phases in the area where no displacement is seen (shown in Fig. 4) is set to zero as a reference.
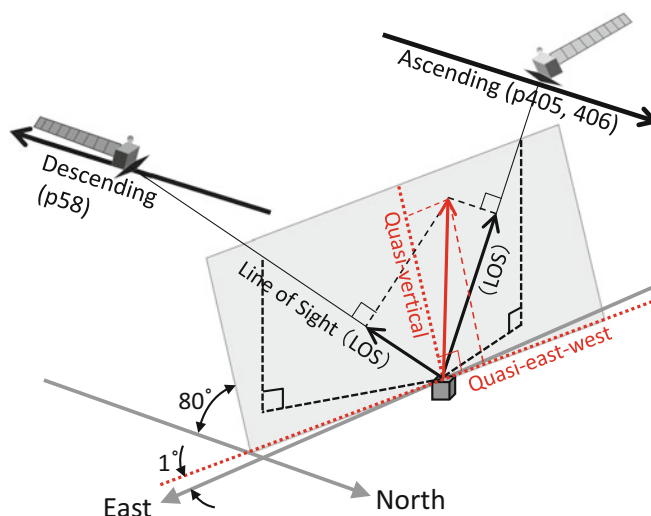

Fig. 3 Schematic diagram of quasi-vertical displacement analysis. The red arrow indicates a displacement vector obtained from and explaining two (ascending and descending) LOS displacements on a plane determined by the two LOS directions. The reason why not "pure" but "quasi-" vertical and east–west components are obtained is that the plane is slightly tilting to the south and horizontally rotating

Table 1 ALOS/PALSAR datasets used for PSI analysis in this study

Path	Row	Orbit	Data set number	Offnadir angle
405	700–710	Ascending	24	34.3°
406	700–710	Ascending	22	34.3°
58	2890–2990	Descending	23	34.3°

4 Results and Discussion

Figure 4 shows the distribution map of quasi-vertical displacement rates (V_v, Fig. 3) from paths 405 and 58. The quasi-vertical displacement rates represent the true vertical ones because no large north–south displacement seems to exist in this area. This figure shows those areas are undergoing strong subsidence (colored in blue and light blue) as well as those areas that are more stable (colored in orange and red). The spatial distribution of the strongly subsiding area was approximately consistent with the results obtained from ENVISAT data by Deguchi et al. 2009. Figure 5a, b shows results overlain on (a) a geomorphological map and on (b) the topographic map of the valley-fill base [Komatsubara et al. 2014] of this area, respectively. As shown in Fig. 5a, almost all the subsidence points, which are indicated by blue and light blue squares, are located within the backmarsh area. In contrast, we confirm that the stable points, indicated by red and orange squares, are distributed across the natural levees (hatched with dotted symbols) and in some parts of

Fig. 4 Average rates of quasi-vertical displacement (V_v) and a reference point (35.920N, 139.773E) in the study area
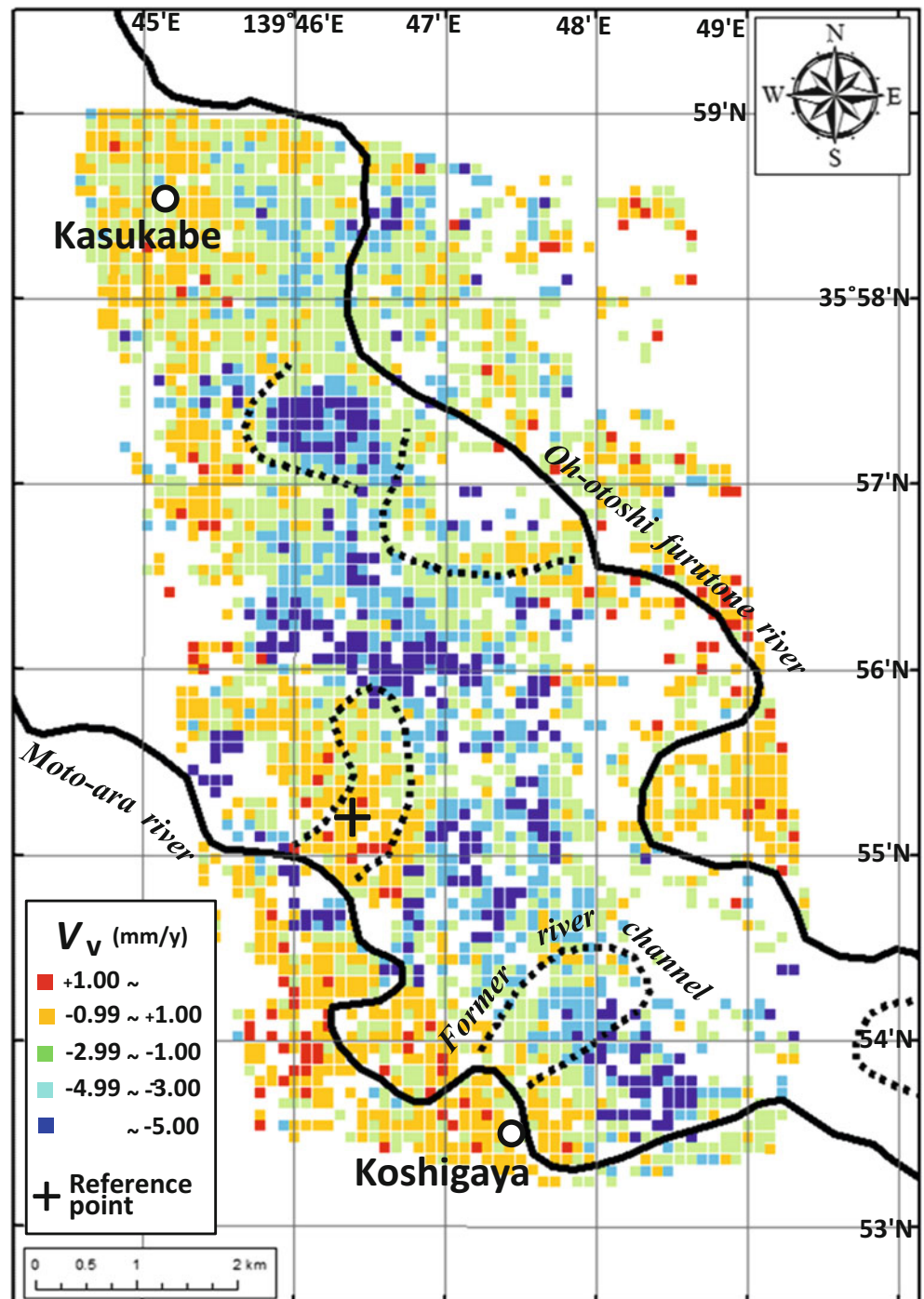
the backmarsh (hatched with horizontal thin lines), indicated as zones A, B, C and D. On the basis of Fig. 5b, we confirm that zones A-D are located above the buried terraces which are distributed around −20 m in elevation. Further,

it can be seen that the subsidence areas, whose average displacement rates exceed 10 mm/year, are distributed along the western margin of the buried valley bottom, as well as in the backmarsh area near the surface. It should be noted
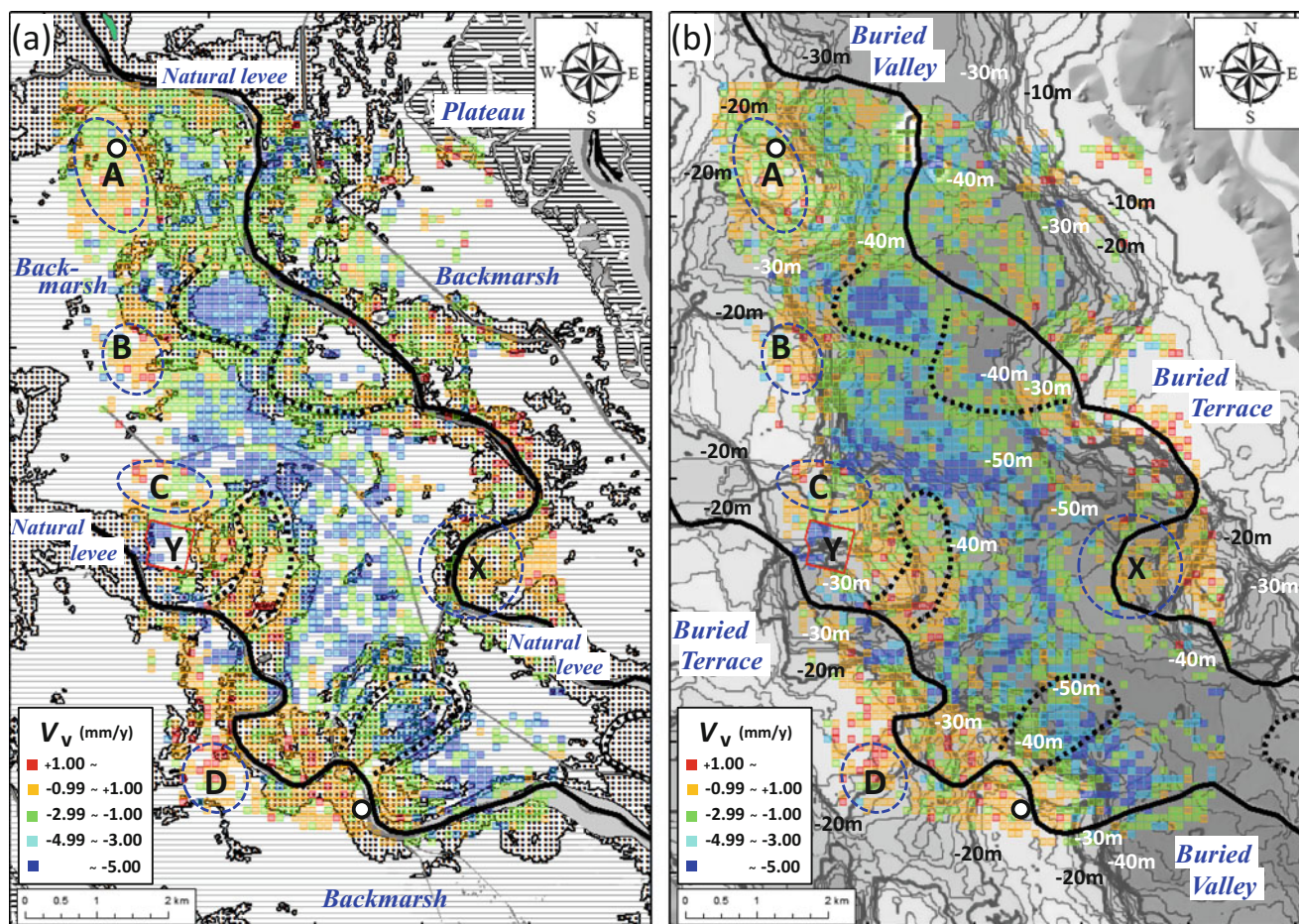
Fig. 5 Average rates of quasi-vertical displacement (V_v) on (**a**) a geomorphological map, and (**b**) a topographic map of the valley-fill base [Komatsubara, 2014] in the study area. The base map was made base on the land condition map "Noda" and "Omiya" (GSI)

Table 2 Sedimentary system and lithofacies of the latest Pleistocene to Holocene incised-valley fills under the central part of Nakagawa lowland [from Nakanishi et al. 2011]

Depositional system	Sedimentary facies	Lithofacies	Elevation (m)	
			Min.	Max.
Delta	Modern river floodplain	Mud	+5	−30
	Modern river channel	Sand		
	Salt marsh and shallow marine	*Mud*		
Estuary	*Tidal influenced shallow marine*	*Mud*	−25	−35
	Tidal flat	*Mud*		
Meandering river	*Meandering river floodplain*	*Mud*	−30	−40
	Meandering river channel	Sand		
Braided river	Braided river channel	Gravel	−35	−45

that some areas inside the buried valley are stable, such as zone X, but almost all of these areas are located on natural levees according to the land classification shown in Fig. 5a. The incised-valley fills under the Nakagawa lowland were formed during the last glacial age [Kimura et al. 2006; Tanabe et al. 2008]. The alluvial sediments are classified into

the following seven facies in ascending order: Braided river channel fills; meandering river floodplain sediments; tidal flat sediments; tide-influenced transgressive shallow marine sediments; upward-shallowing marine sediments; salt marsh sediments; and modern river channel fill and floodplain sediments (Table 2) [Nakanishi et al. 2011]. The braided

Fig. 6 Average rates of LOS displacement (V_{LOS}) given by PSI analysis in the area surrounding the strongest subsidence zone (zone Y). (PSI data: P406/R700-710)
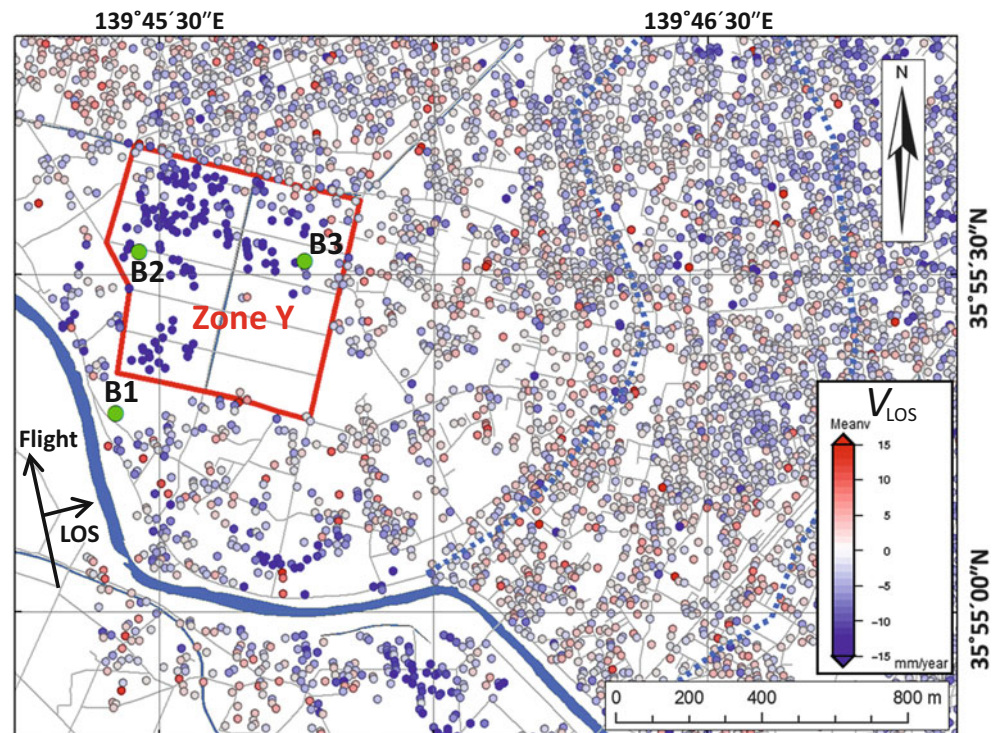
river channel fills consist of gravels that are 2–3 cm in diameter, which form the basis of a good aquifer in this area. The meandering river floodplain sediments lie just above the aquifer, and consist of silt with plant fragments and fine sand. Thus, it suggests that withdrawal of groundwater from the gravel layer which is distributed around −40 m in elevation triggered downward motion of the mud layers right above the gravel layer.

In addition, we detected strong subsidence with an average displacement rate exceeding 15 mm/year above the buried terraces in the western margin of the study area, shown by zone Y in Figs. 5 and 6. Figure 6 shows the PSI analysis results from path406, between August 2006 and April 2011. It is clear that the zone Y shows a remarkable subsidence tendency compared with the surrounding area. Figure 7 illustrates drill logs with N-values provided by the standard penetration test (SPT N-values) in zone Y. In Fig. 6, the average rate of LOS displacement at the B3 site is larger than that at the B1 site. However, the thickness of the unconsolidated silt layer at the B3 site is thinner than at the B1 site. Therefore, we estimate that the most

significant subsidence occurred in the layer shallower than 15 m beneath the ground surface in this area. Figure 8a, b illustrates temporal changes in land use within zone Y. Figure 8a shows the land use situation 11 years before the SAR data acquisition. From this figure, we can confirm that paddy fields were distributed across the entire area of zone Y. Thus, on the basis of Figs. 7 and 8a, it is clear that an unconsolidated silt layer is distributed thickly beneath the surface in this area, and that the groundwater level exists a depth of around 1 m. Figure 8b shows the land use distribution 4 years before the SAR data acquisition. This shows that the construction of urban developments had begun and that a regulating reservoir had been built to the south. Generally, when construction takes place on soft ground, civil engineers preempt any land subsidence by preloading the ground and pumping up the groundwater. In this study area, it is supposed that preconsolidation of the shallow ground was carried out by the preloading of landfills and the drainage of shallow groundwater by the regulating reservoir. Hence, it is assumed that the strongest subsidence detected by the PSI analysis in zone Y is a phenomenon related to

Fig. 7 Drill logs with SPT
N-values around zone Y. GL:
elevation of ground surface, GW:
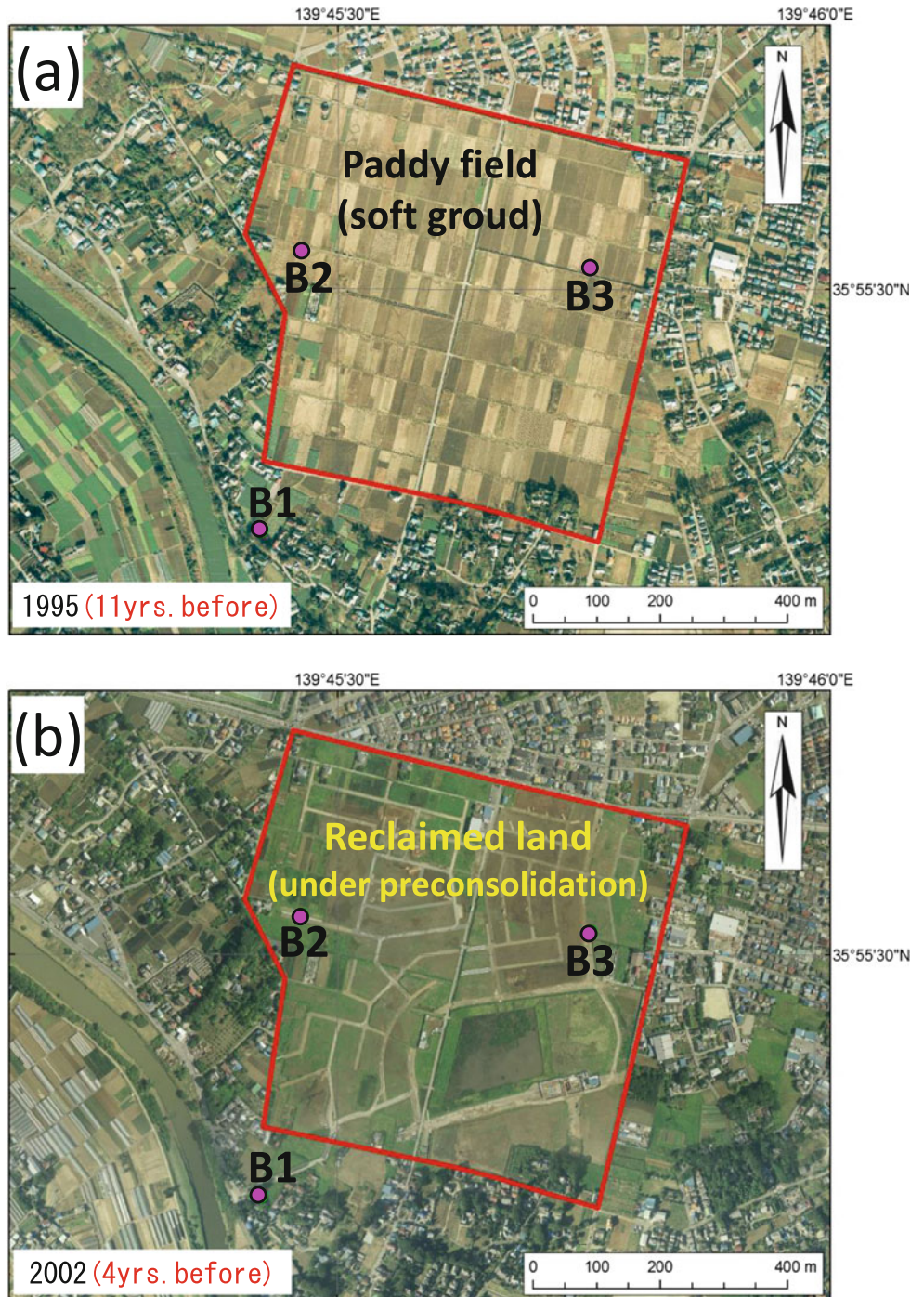elevation of groundwater
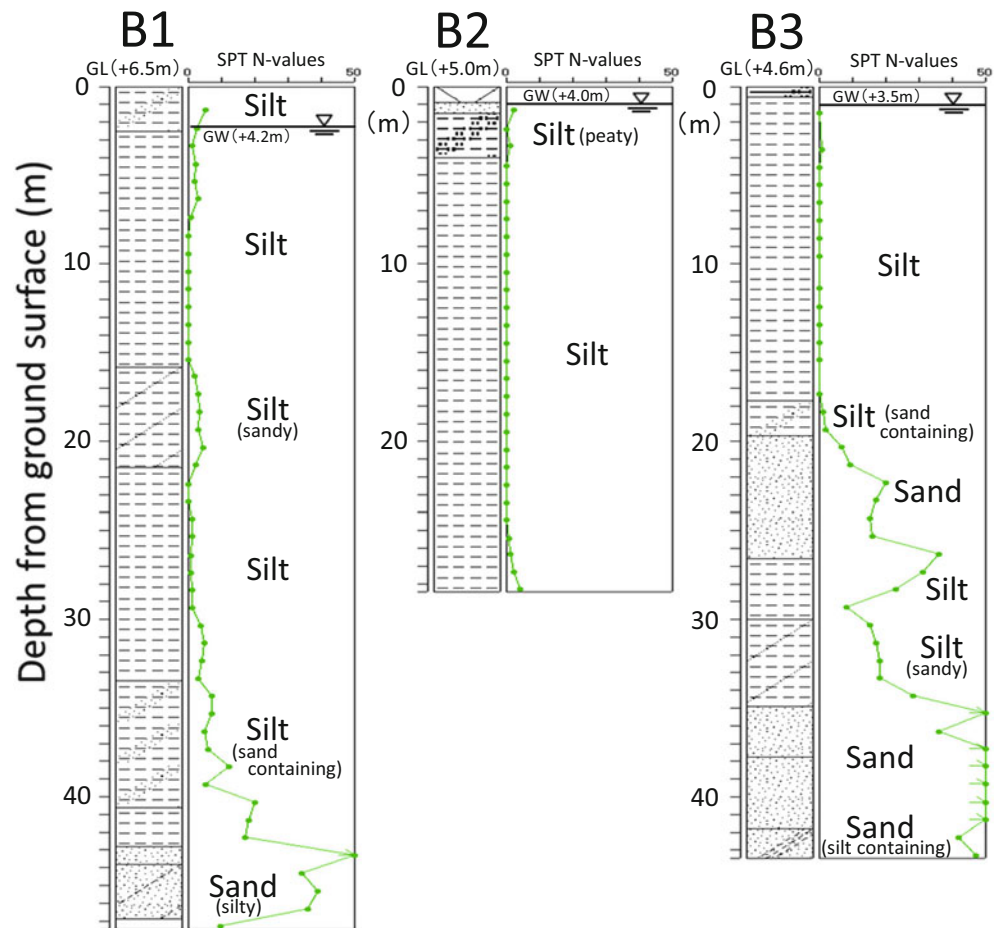
the final stage of preconsolidation during construction upon
reclaimed land.

5   Conclusions

In the Kanto Plain, subsidence areas, with average displace-
ment rates exceeding 10 mm/year, are distributed along the
western margin of a buried valley bottom (from −40 m to
−50 m in elevation) and on the backmarsh near the surface.
These subsidence zones are believed to be caused by the
presence of a geological structure of valley fills beneath the
alluvial plain and by groundwater pumping that targets the
basal gravel layer at the bottom of the valley fills. Average
displacement rates exceeding 15 mm/year were detected
in a patchy zone (zone Y: Approximately 0.3 km^2), and
likely occurred as a result of consolidation settlement on soft
ground following preloading by residential landfill.

Fig. 8 Land use situation in 1995 to 2002 at zone Y (Aerial photos: (**a**) Saitama Pref. 1995-A-33B-54, (**b**) Saitama Pref. 2002)

References

Bekaert DPS, Hooper A, Wright TJ (2015) Reassesing the 2006 Guerrero slow-slip event, Mexico: implications for large earthquakes in the Guerrero Gap. J Geophys Res Solid Earth 120:1357–1375. doi:10.1002/2014JB011557

Constan A, Armenteros AM, Fernandez F, Rosillo S, Delgado JM, Bekaert DPS, Sousa JJ, Gil AJ, Cuenca MC, Hanssen RF, Zaldivar J, Galdeano CS (2016) Multi-temporal InSAR evidence of ground subsidence induced by groundwater withdrawal: the Montellano aquifer (SW Spain). Environ Earth Sci 75:242. doi:10.1007/s12665-015-5051-x

Deguchi T, Rokugawa S, Matsushima J (2009) Long-term ground deformation measurement by time series analysis for SAR interferometry. J Remote Sens Soc Japan 29:418–428 (in Japanese with English abstract)

Endo T (2009) Historical review of groundwater withdrawal management in the southern Kantoh Regions with reference to one by the Tokyo Metropolitan Government. Proc Symp Jpn Soc Eng Geol 1–25 (in Japanese)

Ferretti A, Prati C, Rocca F (2000) Nonlinear subsidence rate estimation using permanent scatterers in differential SAR interferometry. IEEE Trans Geosci Remote Sens 38(5):2202–2212

Fujiwara S, Nishimura T, Murakami M, Nakagawa H, Tobita M, Rosen PA (2000) 2.5-D surface deformation of M6.1 earthquake near Mt Iwate detected by SAR interferometry. Geophys Res Lett 27:2049–2052

Hachinohe S, Hayashi T, Wada E, Osada M (2014) Ground of Saitama prefecture. In: Shin Kanto no Jiban. Maruzen Co Ltd., Japanese Geotechnical Society, pp 81–96 (in Japanese)

Hayashi T (2004) Change of groundwater environment and groundwater quality in the central part of the Kanto plain. J Jpn Assoc Hydro Sci 34:217–226 (in Japanese with English abstract)

Hooper A, Bekaert D, Spaans K, Arikan M (2012) Recent advances in SAR interferometry time series analysis for measuring crustal deformation. Tectonophysics 514–517:1–13. doi:10.1016/j.tecto.2011.10.013

Huang M-H, Tung H, Fielding E, Huang H-H, Liang C, Huang C, Hu J-C (2016) Multiple fault slip triggered above the 2016 Mw 6.4 MeiNong earthquake in Taiwan. Geophys Res Lett 43:7459–7467. doi:10.1002/2016GL069351

IPCC (2013) Climate change 2013: the physical science basis. In: Stocker TF et al (eds) Contribution of Working Group I to the Fifth Assessment Report of the Intergovernmental Panel on Climate Change. Cambridge University Press, Cambridge, United Kingdom and New York, NY, USA, p 1535

Ishitsuka K, Fukushima Y, Tsuji T, Yamada Y, Matsuoka T, Giao PH (2014) Natural surface rebound of the Bangkok plain and aquifer characterization by persistent scatterer interferometry. Geochem Geophys Geosyst 15:965–974. doi:10.1002/2013GC005154

Japan Meteorological Agency (2013) Global Warming Projection 8: 88 (in Japanese)

Kampes B, Hanssen R, Perski Z (2003) Radar interferometry with public domain tools. Proc. Fringe 2003, p 6

Kimura K, Ishihara Y, Miyachi Y, Nakashima R, Nakanishi T, Nakayama T, Hachinohe S (2006) Sequence stratigraphy of the latest Pleistocene-Holocene incised valley fills from the Tokyo and Nakagawa Lowland, Kanto Plain, central Japan. Mem Geol Soc Jpn 59:1–18 (in Japanese with English abstract)

Kobayashi T, Ishimoto M, Tobita M, Yarai H (2014) A tool for reduction of atmosphere-related noises included in an InSAR image, incorporating a numerical weather model. Bull GSI 125:31–38 (in Japanese)

Kobayashi T, Morishita Y, Yarai H (2015) Detailed crustal deformation and fault rupture of the 2015 Gorkha earthquake, Nepal, revealed from ScanSAR-based interferograms of ALOS-2. Earth Planets Space 67:201. doi:10.1186/s40623-015-0359-z

Komatsubara J (2014) Basal topography of the latest Pleistocene – Holocene valley fills under the Arakawa Lowland, Nakagawa Lowland and Tokyo Lowland, central Japan. In: Integral research and application of the subsurface geology "the central Kanto Plain", Miscellaneous Map Series. Geol. Surv. Japan, vol 40, AIST, pp 51–55 (in Japanese with English abstract)

Morita M (2015) Present state of land subsidence in the northern Kanto Plain. J Groundwater Hydrol 57:29–36 (in Japanese)

Nakanishi T, Tanabe S, Kimura K, Nakashima R, Uchiyama M, Shibata Y (2011) Sedimentary facies, diatom assemblages, physical properties and radiocarbon ages of the latest Pleistocene to Holocene incised valley fills under the central area of the Nakagawa Lowland, Kanto Plain, central Japan. Bull Geol Surv Jpn 62:47–84 (in Japanese with English abstract)

Ozawa T, Fujita E (2013) Local deformations around volcanoes associated with the 2011 off the Pacific coast of Tohoku Earthquake. J Geophys Res 118:390–405. doi:10.1029/2011JB009129

Tanabe S, Nakanishi T, Kimura K, Hachinohe S, Nakayama T (2008) Basal topography of the Alluvial under the northern area of the Tokyo Lowland and Nakagawa Lowland, central Japan. Bull Geol Surv Japan 59(11/12):497–508 (in Japanese with English abstract)

Tobita M, Munekane H, Matsuzaka S, Kato M, Yarai H, Murakami M, Fujiwara S, Nakagawa H, Ozawa T (2005) Studies on InSAR data processing technique. J Geospatial Inf Auth Jpn 106:37–49 (in Japanese)

Zebker HA, Rosen PA, Goldstein RM, Gabriel A, Werner CL (1994) On the derivation of coseismic displacement fields using differential radar interferometry: the Landers earthquake. J Geophys Res 99(B10):19617–19634